The impact of chronic kidney disease on arteriovenous fistula remodeling: studies in a murine model of autosomal dominant polycystic kidney disease

Laboyrie, S.L.; Peters, D.J.M.; Bijkerk, R.; Winter, E.P. de; Duijs, J.M.G.J.; Klerk, J.A. de; ... ; Rotmans, J.I.

AMERICAN JOURNAL OF PHYSIOLOGY
RENAL PHYSIOLOGY

Am J Physiol Renal Physiol 329: F453–F464, 2025.
First published August 18, 2025; doi:10.1152/ajprenal.00354.2024

RESEARCH ARTICLE

The impact of chronic kidney disease on arteriovenous fistula remodeling: studies in a murine model of autosomal dominant polycystic kidney disease

Suzanne L. Laboyrie,[1] Dorien J. M. Peters,[2] Roel Bijkerk,[1] Eduard Pierre de Winter,[3] Jacques M. G. J. Duijs,[1] Juliette A. de Klerk,[1] Margreet R. de Vries,[3,4]* and Joris I. Rotmans[1]*

[1]*Department of Internal Medicine, Leiden University Medical Centre, Leiden, The Netherlands;* [2]*Department of Human Genetics, Leiden University Medical Centre, Leiden, The Netherlands;* [3]*Department of Surgery, Leiden University Medical Centre, Leiden, The Netherlands; and* [4]*Department of Surgery, Brigham & Women's Hospital, Harvard Medical School, Boston, Massachusetts, United States*

Abstract

The arteriovenous fistula (AVF) is the gold standard for hemodialysis vascular access, although inadequate vascular remodeling and intimal hyperplasia pose a major limitation. It is essential to study this in a clinically relevant model. We used an autosomal dominant polycystic kidney disease (ADPKD) model, the most common hereditary cause of chronic kidney disease (CKD), to study the effect of CKD on AVFs. Jugular-carotid AVFs were created in adult *B6OlaPkd1*$^{nl/nl}$ (ADPKD) mice and *B6OlaPkd1*$^{+/+}$ littermates. AVFs were harvested 7 days postsurgery for bulk mRNA sequencing or 3 wk postsurgery for histological analysis. We performed weekly AVF flow measurements using Doppler ultrasound and assessed kidney morphology and function by histology and blood urea analysis. Blood pressure was measured using a tail cuff, before and 6 days after AVF surgery. Longitudinal flow data was analyzed using mixed-effects model, histological data using the Mann–Whitney *U* test. *Pkd1*$^{nl/nl}$ mice developed cystic kidneys and elevated blood urea levels (8.7 ± 2.8 mmol/L vs. 24.0 ± 3.8 mmol/L) and higher mean arterial blood pressure (92 vs. 113). AVF flow in *Pkd1*$^{nl/nl}$ mice was consistently higher post-AVF creation (1.9-fold difference, $P < 0.001$), with a 50% reduction in intimal hyperplasia and 30% increase in luminal AVF volume. RNA sequencing showed altered regulation of extracellular matrix in the venous ADPKD AVF, with reduced collagen deposition in the venous outflow tract. The arterial AVF wall had disruption of the elastic laminae. *Pkd1*$^{nl/nl}$ mice are a suitable model to study AVF remodeling in a CKD setting, resulting in enhanced luminal volume and higher AVF flow when compared with normotensive mice with normal kidney function.

NEW & NOTEWORTHY This work explores the impact of chronic kidney disease (CKD) on arteriovenous fistula (AVF) remodeling using an autosomal dominant polycystic kidney disease (ADPKD) mouse model. Our findings reveal that ADPKD enhances AVF flow and luminal volume while reducing intimal hyperplasia, due to altered extracellular matrix deposition, offering new insights into the vascular AVF changes in a CKD setting. This study highlights the suitability of the ADPKD model for investigating AVF remodeling in a CKD context.

arteriovenous fistula; autosomal dominant polycystic kidney disease; chronic kidney disease; murine model; vascular remodeling

INTRODUCTION

To optimize the efficacy of hemodialysis treatment for end-stage kidney failure (ESKD), a well-functioning vascular access site providing a robust blood flow supply to the dialyzer is essential. Although the arteriovenous fistula (AVF) is the preferred vascular access method, its frequent primary failure poses a significant challenge. Factors such as inadequate outward remodeling (OR) and the occurrence of excessive stenosis or intimal hyperplasia (IH) can hinder AVF maturation, creating a bottleneck for initiating hemodialysis (1). These vascular access-related complications lead to hospitalizations, increased morbidity, and impose a substantial burden on both patients and health care. Therefore, comprehending the process of AVF maturation failure and understanding how factors like kidney failure influence vascular remodeling post-AVF surgery is crucial.

To investigate the impact of the uremic environment on AVF vascular remodeling, studies have predominantly utilized models of acute kidney failure, such as nephrectomy (2–4) or unilateral ureteral obstruction (5), L-NAME administration to induce vascular injury and hypertension (6), or diet-induced kidney failure.(7, 8) However, these acute kidney injury models fail to replicate the phenotype of ESKD, lacking the aspects of early onset kidney

*M. R. de Vries and J. I. Rotmans contributed equally to this work.
Correspondence: J. I. Rotmans (j.i.rotmans@lumc.nl).
Submitted 10 December 2024 / Revised 22 January 2025 / Accepted 4 August 2025

injury, the progressive injury associated with ESKD and hypertension—key clinical characteristics observed in many ESKD patients receiving an AVF. Consequently, a representative ESKD model for studying its effect on AVF maturation is currently lacking. However, as hypertension is argued to have a protective effect on AVF failure (9, 10), whereas uremia accelerates wall thickening and IH in mice (3, 11), it is important to incorporate both these ESKD hallmarks in one model to study AVF maturation.

In the present study, we used a clinically relevant CKD model to elucidate the impact of CKD on vascular AVF remodeling. Specifically, we utilized a well-characterized murine model of autosomal dominant polycystic kidney disease (ADPKD) (12, 13), the most common hereditary cause of kidney failure, and created AVFs between the carotid artery and jugular vein.

Our analysis included the evaluation of kidney function and blood pressure and investigating the effects of CKD on blood flow and vascular remodeling in the AVF. Acute kidney injury models showed that kidney failure mainly affected AVF remodeling through IH aggravation (3, 11). We however hypothesized that our chronic CKD model, along with its impact on blood pressure and progressive vascular damage, affects AVF maturation mostly through medial vessel wall turnover.

MATERIALS AND METHODS

Animals and Study Design

This study was performed in compliance with Dutch guidelines, the Directive 2010/63/EU of the European Parliament, and was approved by the Institutional Committee for Animal Welfare at the Leiden University Medical Center. Adult *B6Ola-Pkd1*$^{+/+}$ and *B6Ola-Pkd1*$^{nl/nl}$ mice, aged 8 to 12 wk and bred in our own facility, were used for the in vivo studies. We decided on a minimal sample size using G*power calculation, where we viewed intimal hyperplasia as the main parameter. The study groups were littermates and were housed together. Every surgery session was performed blinded, and mice of the same cage—i.e., possibly both *B6Ola-Pkd1*$^{+/+}$ and *B6Ola-Pkd1*$^{nl/nl}$ mice—received an AVF to minimize confounding. Due to ADPKD's genetic background, the animals could not be randomized, instead the two groups were matched for age and sex. Heterozygous littermates were excluded from the study.

The previously described ADPKD model (12, 13) with an intronic neomycin-selectable marker causing aberrant splicing of intron 1 has a hypomorphic Pkd1 allele. This results in reduced (10%–20%) *Pkd1* transcript levels in kidneys of *B6Ola-Pkd1*$^{nl/nl}$ mice compared with their wildtype *B6Ola-Pkd1*$^{+/+}$ controls. Before AVF surgery, the mice were anesthetized via intraperitoneal injection of midazolam (5 mg/kg, Roche), medetomidine (0.5 mg/kg, Orion), and fentanyl (0.05 mg/kg, Janssen) and received unilateral AVFs, as previously described (14) between the dorsomedial branch of the external jugular vein and the common carotid artery (CCA). After surgery, anesthesia was antagonized with atipamezole (2.5 mg/kg, Orion) and flumazenil (0.5 mg/kg, Fresenius Kabi). Buprenorphine (0.1 mg/kg, MSD Animal Health) was given after surgery for 2 days to relieve pain.

It should be noted that compared with previously used models on a C57BL/6 or B6.129S2 background (14, 15), we observed some challenges with anesthetizing the animals before surgery, with delayed subconsciousness and rapid recovery from anesthesia. Therefore, adequate monitoring of the level of anesthesia presurgery through toe pinching was performed throughout surgery, and in some individuals, additional anesthesia was provided during surgery.

Before AVF surgery, blood pressure was measured in six *Pkd1*$^{+/+}$ and six *Pkd1*$^{nl/nl}$ mice, and in the same animals 6 days post-AVF surgery. All mice underwent Doppler ultrasound at baseline, *day 3* post surgery and then weekly. During AVF surgery (*day 0*) and tissue harvest at *day 21*, blood was retrieved to measure blood urea levels. We assessed vascular remodeling both at the early stage, 7 days post-AVF surgery, through RNA sequencing, to investigate which processes preceded the eventual stable phase 21 days post-AVF surgery, which we assessed with histology. Kidneys from all mice were harvested to monitor cyst formation. The experimental protocol is shown in Fig. 1.

Blood Pressure Measurements

Systolic and diastolic blood pressure were assessed with a noninvasive tail cuff system in conscious mice using the CODA system (Kent Scientific, Torrington, CT, USA). To minimize stress, blood pressure and ultrasound analysis were measured on separate days. Blood pressure was measured according to the manufacturer's instructions 2 days before the AVF surgery and 6 days postsurgery. Animals were acclimated to the restrainer before measurements. Hereafter, 10 acclimation cycles were followed by 20 measurement cycles.

Blood Urea Measurements

Blood was obtained from the AVF at its creation, using Lithium Heparin capillary tubes (Abbott No. 52193), and at euthanize, 21 days after surgery. Blood urea levels were determined with Reflotron Urea strips (Roche diagnostics, No. 11200666202) on the Reflotron Plus (Roche Diagnostics, Basel, Switzerland) according to the manufacturer's protocol.

RNA Isolation and RNA Sequencing

Seven days post-AVF surgery, five mice per group were anesthetized as described previously and perfused with PBS through cardiac perfusion. AVFs were collected and separated into the arterial and venous segments, which were snap frozen in liquid nitrogen. RNA was isolated using the Qiagen RNeasy microkit (74004) according to the manufacturer's protocol with several adjustments: adding 1% β-mercaptoethanol to the RLT lysis buffer, performing tissue disruption and homogenization with glass beads at 1,800 rpm for 1 min, followed by proteinase K digestion for 10 min at 55°C. After quality control of the RNA, this resulted in $n = 4$ for wild-type venous AVF samples and $n = 5$ for venous AVF samples from *Pkd1*$^{nl/nl}$ mice. The arterial AVF samples were $n = 3$ for *Pkd1*$^{+/+}$ and $n = 4$ for *Pkd1*$^{nl/nl}$ mice. Preparation and bulk mRNA

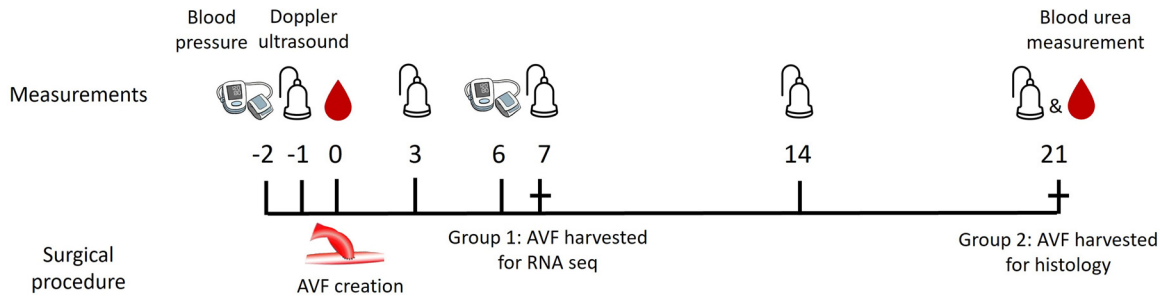

Figure 1. Experimental protocol of murine AVF studies. AVF, arteriovenous fistula; RNA seq, bulk RNA sequencing.

sequencing were performed at Genomescan (Leiden, The Netherlands), with 20 million PE150 reads. Total RNA was quantified and ≥250 ng was used as input on the Illumina NovaSeq6000.

Differential Gene Expression Analysis

Differentially expressed genes (DEGs) between AVF samples, both arterial and venous, harvested 7 days after surgery of *Pkd1*$^{+/+}$ and *Pkd1*$^{nl/nl}$ mice were identified. Reads were aligned to the mouse genome (GRCm39 M33) with STAR (v2.7.7a). For the assessment of differential expression, a quasi-likelihood negative binomial generalized log-linear model was used, using *R* package edgeR (v3.42.4). Counts underwent normalization through the Trimmed Mean of the M-values (TMM) method. Genes were considered differentially expressed if the observed contrast between ADPKD and controls reached statistical significance, as indicated by a false discovery rate (FDR)-adjusted *P* value below 0.05. Gene set enrichment analysis was performed with *R* package clusterProfiler (v.4.8.3) of gene ontology (https://geneontology.org/). All analyses were performed using *R* statistics (v4.3.1). Figures were produced using the *R* packages ggplot2 (v3.4.4) and enrichplot (v.1.20.3), showing the data as counts per million (cpm).

Ultrasound Analysis and 3-D Volume Measurements

Ultrasound analysis was performed under isoflurane anesthesia as described previously (15) 1 day before AVF surgery, and at *days 3* and *7* post-AVF creation for every animal, and *day 14* and *21* for mice that were euthanized at 21 days after surgery. The following recordings were obtained at each time point: ECG-gated Kilohertz visualization (EKV) brightness-mode (B-mode) of the CCA afferent to the anastomosis, short-axis three-dimensional B-mode and color Doppler, long-axis three-dimensional B-mode and color Doppler, PW Doppler of the CCA afferent to the anastomosis. For the PW Doppler measurements, an angle of ≤59° was used. We extrapolated the diameter and thereby area of the CCA from the EKV measurements, and flow velocity from PW Doppler data. These measurements were used to define flow volume in the AVF: flow volume = $(\text{CCA diameter}/2)^2 \times \pi \times$ mean flow velocity. Maximum systolic accelerations (ACCmax) were measured from PW Doppler data.

Luminal volumes of the AVFs were measured by tracing the lumen downstream of the anastomosis in the first 63 frames, each 0.04 mm apart, directly in the short-axis three-dimensional B-mode. The length of the AVF in the selected frames was also measured, using the measuring tool in VEVO laboratory and mid-lumen points of the traced areas. The total volume was then corrected for the total length of the AVF, allowing for the appreciation of the volume in the AVF over the first 2.5 mm downstream of the anastomosis.

Tissue Harvest and Processing for Histology

Twenty-one days after AVF surgery, mice were anesthetized using a mixture containing midazolam (5 mg/kg, Roche), medetomidine (0.5 mg/kg, Orion), and fentanyl (0.05 mg/kg, Janssen) via intraperitoneal injection. The thorax was opened and flushed through intracardiac perfusion with PBS and thereafter formalin, whereafter the AVF and kidneys were dissected and submerged in formalin overnight, then embedded in paraffin. Since most AVF remodeling occurs in the venous outflow tract of the AVF, the first three perpendicular venous cross sections downstream of the anastomosis with 150-µm interval were used for morphological and immunohistochemical analysis.

Second Harmonic Generation

Paraffin-embedded tissue was deparaffinated and rehydrated. Tissue sections (5 µm) were excited with a laser using an 800 nm wavelength using Multiphoton microscopy (Zeiss LSM 710). Second harmonic generation (SHG) images were obtained using a band-pass emission filter at the SHG (380–430 nm) wavelength. A wide-band pass emission filter (300–755 nm) was also used to collect the combined all two-photon excited fluorescence (TPF) signal. Collagen quantification was performed with ImageJ software by calculating the SHG-positive area over the total vessel area.

Staining and Morphometric Analysis

Kidneys were stained using Periodic acid-Schiff (PAS) staining. To verify RNA-sequencing findings at 21 days post-AVF surgery, murine AVFs were stained for Tenascin-C (Sigma Aldrich, ZRB2975) and VEGFR3 (Abcam ab317030), which is encoded by Flt4.

Murine AVFs were stained with Weigert's elastin to visualize the elastic lamina of the venous outflow tract and CCA afferent to the anastomosis. Tissue within the internal elastic lamina (IEL) of the venous AVF outflow tract

was defined as IH and determined using histoquant software (3DHISTECH). Slides that were used to study collagen deposition were analyzed with SHG and followingly stained for αSMA (DAKO M0851) and Vimentin (Thermo Scientific, MS-129-P1) to determine presence of collagen-producing cells.

Morphology of Extracellular Matrix in Human Renal Arteries

To evaluate whether the observations in our mouse model corresponded to patient blood vessels, renal arteries were obtained post nephrectomy. We included two patients with renal cell carcinoma with normal kidney function (control samples) and two patients with ADPKD. Specimens were obtained at the LUMC in accordance with guidelines set out by the "Code for Proper Secondary Use of Human Tissue" of the Dutch Federation of Biomedical Scientific Societies (Federa) and conform with the principles outlined in the Declaration of Helsinki. The study was approved by the local ethical committee, and the donors gave informed consent. The control samples were obtained from donors with an eGFR $>$ 60 mL/min/1.73 m^2. They underwent nephrectomy due to renal carcinoma and did not have metastasis or diabetes mellitus. The arterial samples were used for histological analysis to study the extracellular matrix, using a Weigert's elastin stain and Masson Trichrome staining.

Statistical Analysis

GraphPad Prism 8 was used to perform statistical analysis. Normally distributed data are presented as means ± SD. Nonparametric data are presented as the median ± interquartile range. Unpaired t test, one-way ANOVA, Restricted Maximum Likelihood (REML), and Mann–Whitney *U* test (2-tailed) were used when applicable. $P <$ 0.05 is considered significant. Analyses were also separately performed for male and female mice; results can be found in the Supplemental figures.

RESULTS

Surgical Outcome

Thirty-six animals received an AVF, of which 15% from the *Pkd1*$^{+/+}$ mice and 14% of *Pkd1*$^{nl/nl}$ mice were excluded from morphological analysis due to technical difficulties during surgery, such as vessel spasms or bleeding, causing early occlusion or distorted vascular remodeling of the lumen, as seen on ultrasound analysis observed at early time points such as directly or 3 days post-AVF surgery. Seventeen *Pkd1*$^{+/+}$ (9 females, 8 males) and 19 *Pkd1*$^{nl/nl}$ mice (10 females, 9 males) were included in the study.

Pkd1$^{nl/nl}$ Mice Developed Chronic Kidney Disease and Hypertension

Kidneys of *Pkd1*$^{nl/nl}$ mice were visibly larger in size compared with control mice and presented with cysts throughout the kidneys (Fig. 2, *A* and *B*). Furthermore, impaired kidney function was observed in *Pkd1*$^{nl/nl}$ mice, with elevated blood urea levels at AVF creation (24.0 ± 3.8 mmol/L, Fig. 2*C*), which remained stable over the 3-wk study period (23.1 ± 3.7 mmol/L), compared with *Pkd1*$^{+/+}$ mice (8.7 ± 2.8 mmol/L at AVF creation and 8.3 ± 3.4 mmol/L at 21 days). *Pkd1*$^{nl/nl}$ mice also developed hypertension, with elevated mean arterial blood pressure (MAP) at both timepoints compared with *Pkd1*$^{+/+}$ mice. *Pkd1*$^{+/+}$ mice, demonstrated a 20% (113 vs. 92, $P = 0.00001$) and 30% (100 vs. 76, $P = 0.002$, Fig. 2*D*) increase in MAP presurgery and 6 days post-AVF surgery. The exact systolic and diastolic blood pressure measurements in *Pkd1*$^{+/+}$ mice are shown in Supplemental Fig. S1.

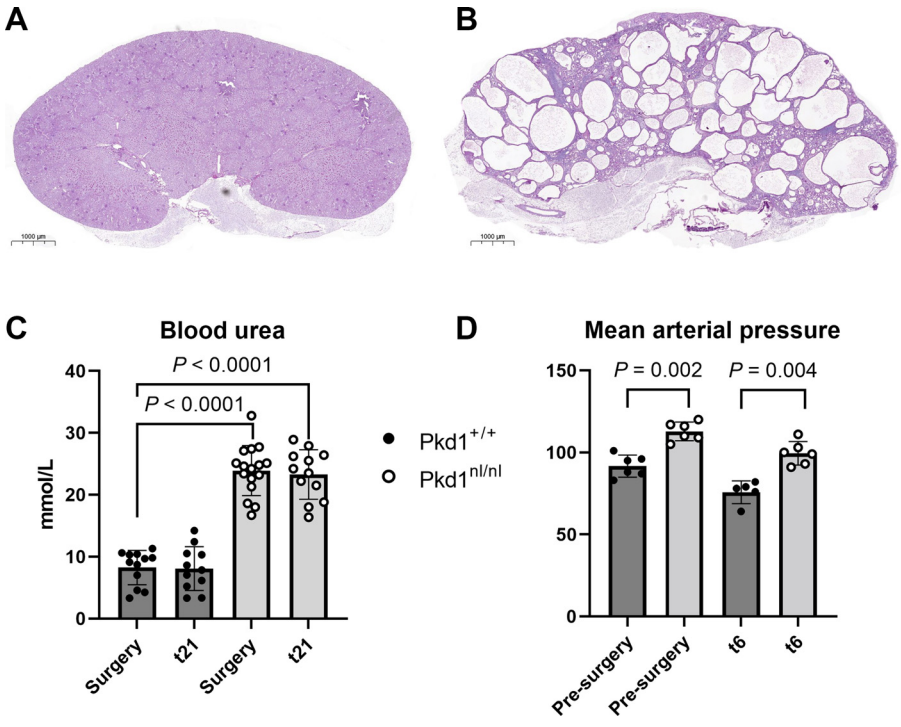

Figure 2. Kidney function and blood pressure in the mouse model. Periodic acid-Schiff (PAS) staining of a healthy *Pkd1*$^{+/+}$ (*A*) and *Pkd1*$^{nl/nl}$ polycystic kidney (*B*). *Pkd1*$^{nl/nl}$ mice have increased blood urea levels throughout the 21-day study period (*C*), and hypertension presurgery and 6 days post-AVF creation (*D*). Data are expressed as means ± SD. ADPKD, autosomal dominant polycystic kidney disease; AVF, arteriovenous fistula.

Venous Disturbed ECM Remodeling in AVFs of *Pkd1*$^{nl/nl}$ Mice

To determine early vascular response and which pathways cascade the vascular remodeling, bulk poly-A RNA sequencing was performed 7 days post-AVF surgery. Differentially expressed (absolute log2 fold change [FC] ≥ 1, adjusted P value ≤ 0.05) processes of vascular remodeling of the arterial AVF segment were mostly related to oxygen exchange and vascular muscle contraction (Supplemental Fig. S2).

The venous outflow tract of AVFs in *Pkd1*$^{nl/nl}$ mice showed several downregulated genes involved in vascular remodeling (*Flt4*, *Tbx1*, *Olfml3*, Fig. 3*A*), and the ECM (extracellular matrix: *Col11A1*, *Tnc*, *Tnn*, and *Acan*). Genes related to mechanical tension (*Palmd*, *Ablim1*) were upregulated. Gene set enrichment analyses of DEGs (Fig. 3*B*) indeed demonstrated transcriptional activation of muscle contraction (vasoconstriction), whereas transcription of processes involved in ECM regulation was inhibited in *Pkd1*$^{nl/nl}$ mice. IPA pathway analysis (Supplemental Table S1) revealed upregulation of transcription factors Gata6, Sox2, Smarca2, Npm1, and Esrra and cytokines CSF1 and IL-13. To verify RNA sequencing findings at 21 days post-AVF surgery, murine AVFs were stained for Tenascin-C and VEGFR3, which is encoded by Flt4 (Fig. 4). Although not statistically significant, we see a similar trend on both *day 7* and *21* post surgery as observed with RNA sequencing, namely, less Tenascin-C and VEGFR3 protein in AVFs of *Pkd1*$^{nl/nl}$ mice compared with *Pkd1*$^{+/+}$ mice.

Pkd1$^{nl/nl}$ Mice Have Increased AVF Flow

Blood flow in the CCA proximal to the site of anastomosis was assessed weekly via ultrasonography. *Pkd1*$^{nl/nl}$ and *Pkd1*$^{+/+}$ mice had comparable flow volume presurgery (Fig. 5*A*), whereafter AVF flow was increased in both groups over the 21-day study period (time, $P < 0.0001$). *Pkd1*$^{nl/nl}$ mice show increased AVF flow volume compared with *Pkd1*$^{+/+}$ mice (group effect, $P = 0.001$), with an increase in both peak and mean blood velocity (Fig. 5*B*) but not increased luminal area of the CCA compared with *Pkd1*$^{+/+}$ mice (Fig. 5*C*). To verify whether hypertension and increased flow velocity in the ADPKD model was caused by vascular stiffness, the maximum acceleration (ACCmax) in the CCA was determined. However, no increase in systolic ACCmax over time nor a group difference between *Pkd1*$^{nl/nl}$ and *Pkd1*$^{+/+}$ mice (Fig. 5*D*) was observed. Male and female mice were also analyzed separately and showed similar differences between *Pkd1*$^{nl/nl}$ and *Pkd1*$^{+/+}$ mice (Supplemental Fig. S3).

Pkd1$^{nl/nl}$ Mice Have Reduced IH and Increased Luminal AVF Volume

To assess the result of the vascular remodeling process at a stable phase, histological and morphological analysis (Fig. 6*A*) of the AVF were performed on samples obtained 21 days post-AVF surgery. The venous outflow tract of the AVF of *Pkd1*$^{nl/nl}$ mice showed a 50% reduction in IH (Fig. 6*B*, $P = 0.03$) and 40% reduction of total vessel wall area (Fig. 6*C*, $P = 0.02$). Ultrasound analysis showed a 28% increase in luminal volume of the venous outflow tract of *Pkd1*$^{nl/nl}$ mice compared to *Pkd1*$^{+/+}$ mice (Fig. 6, *D* and *E*, $P = 0.04$). Sex-specific analyses showed similar trends between *Pkd1*$^{nl/nl}$ and *Pkd1*$^{+/+}$ mice (Supplemental Fig. S4). *Pkd1*$^{nl/nl}$ mice show reduced extracellular matrix deposition in the AVF.

We evaluated the afferent artery for aberrant morphology of the elastic lamina to monitor for potential dilatory effects and the venous outflow tract for collagen deposition. The CCA in *Pkd1*$^{nl/nl}$ mice displayed a reduction in the number of elastic lamina (Fig. 7*A*, $P = 0.002$), despite having similar elastic laminae presurgery. Moreover, the venous AVF outflow tract of *Pkd1*$^{nl/nl}$ mice showed a 2.2-fold decrease in collagen deposition comparatively with

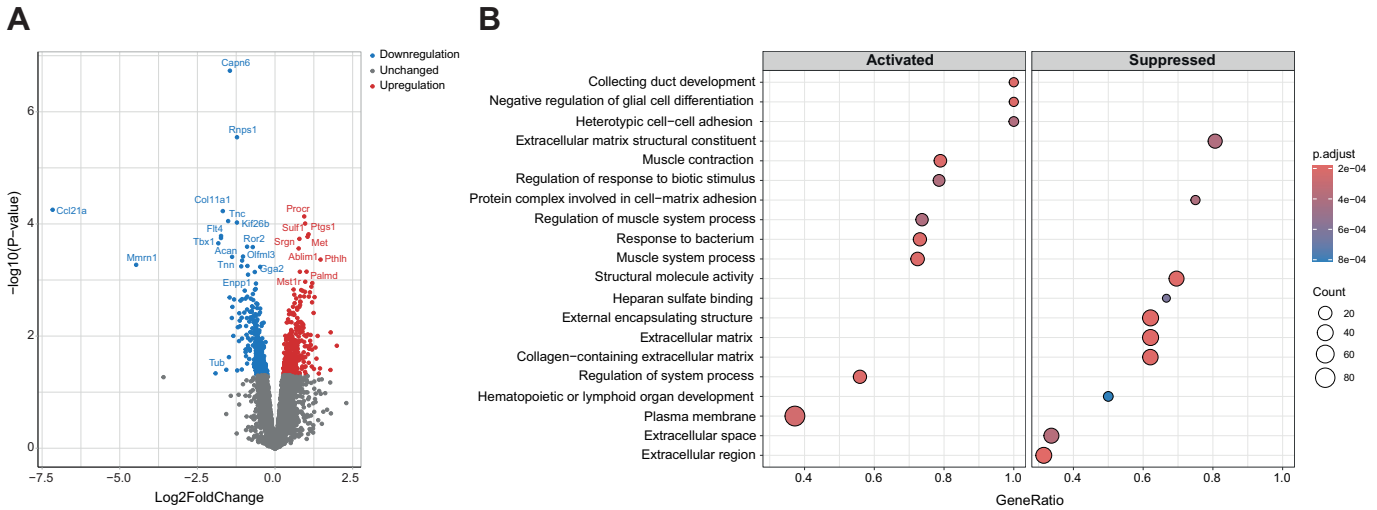

Figure 3. DEGs and functional pathways in the venous c segment. *A*: volcano plot representation of DEGs in the venous AVF outflow tract of *Pkd1*$^{nl/nl}$ mice in pairwise comparisons with *Pkd1*$^{+/+}$ mice. Changes in gene expression are presented as log10 fold change, red dots indicate upregulated genes in AVFs (log2 fold change ≥ 1, adjusted P value < 0.05), and blue dots are genes downregulated in *Pkd1*$^{nl/nl}$ fistulas (log2 fold change ≤ -1, adjusted P value < 0.05). *B*: pathway enrichment analyses of DEGs using gene ontology, showing activated and suppressed biological processes of AVF-induced venous remodeling with *Pkd1*$^{+/+}$ mice as a reference control for gene expression in *Pkd1*$^{nl/nl}$ mice. Gene ratio indicates the ratio of DEGs in an annotated term over all genes in this term. AVF, arteriovenous fistula; DEG, differentially expressed gene.

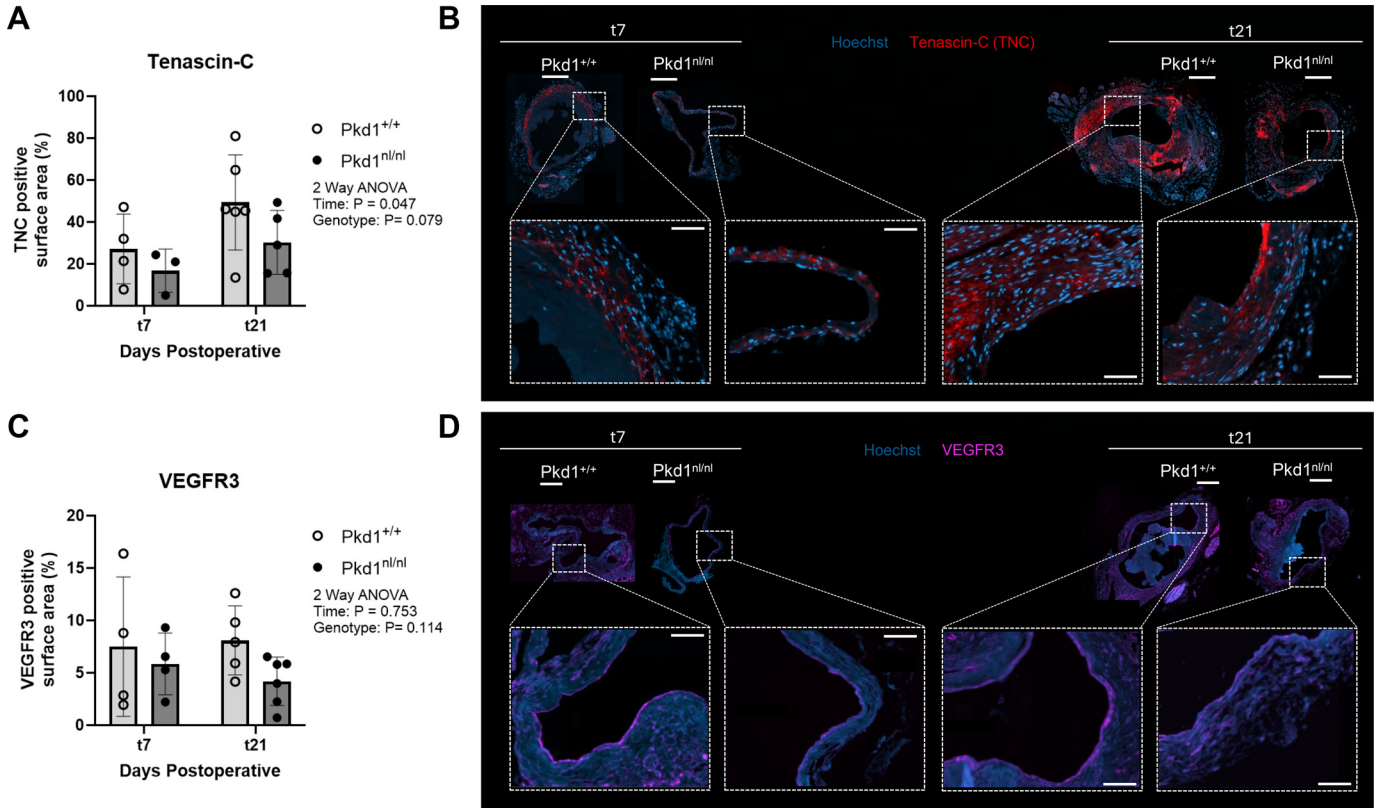

Figure 4. Quantitative analysis of Tenascin-C and VEGFR3. *A*: quantification of Tenascin-C (TNC) in *Pkd1*$^{+/+}$ and *Pkd1*$^{nl/nl}$ AVFs 7 and 21 days postoperatively. *B*: representative images of Tenascin-C quantification. *C*: quantification of VEGFR3 in *Pkd1*$^{+/+}$ and *Pkd1*$^{nl/nl}$ AVFs. *D*: representative images of VEGFR3 quantification. Scale bars represent 200 μm in the full vein images and 50 μm in the magnified *insets*. AVF, arteriovenous fistula.

the vessel wall area (Fig. 7*B*, $P = 0.04$), which could not be explained by a reduction of collagen producing vascular cells (αSMA or Vimentin positive cells, Fig. 7*C*, $P = 0.97$) since comparable values between *Pkd1*$^{nl/nl}$ and controls (median 45% vs. 37%, $P = 0.97$) were observed. Sex-specific analyses showed similar differences in the number of elastic laminae in the CCA and collagen in the vein wall (Supplemental Fig. S5).

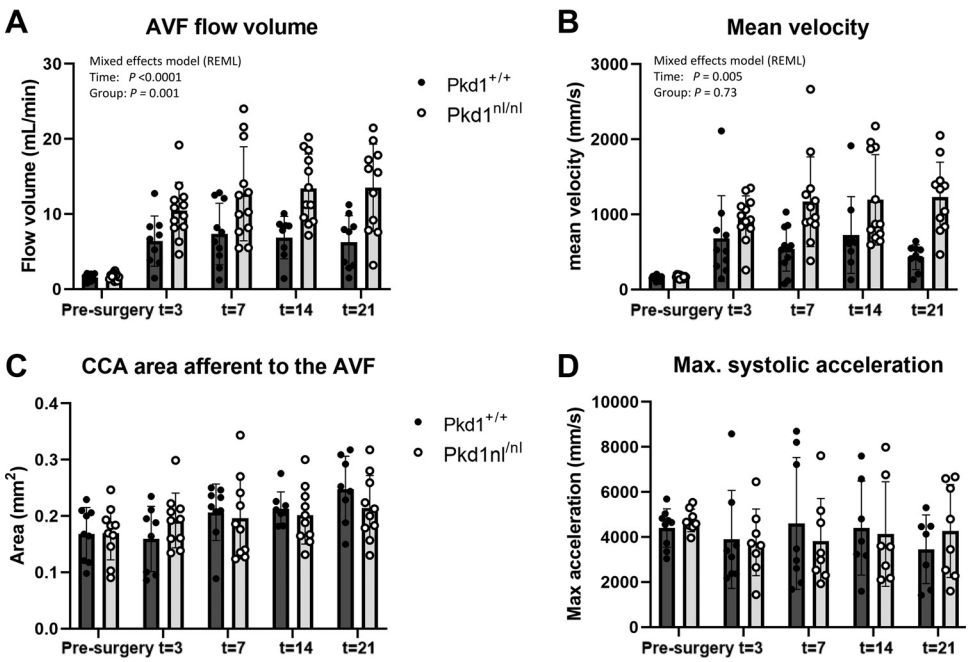

Figure 5. Flow dynamics of the AVF through ultrasound analysis. Blood flow though the AVF increased over time in both groups (*A*), with significantly higher flow in the *Pkd1*$^{nl/nl}$ mice due to increased velocity (*B*). There was no difference in the luminal area of the common carotid artery (CCA) afferent to the AVF anastomosis (*C*) or maximum systolic acceleration (*D*) between the two groups. T represents the number of days post-AVF surgery, data are expressed as means ± SD, n = 12. *Pkd1*$^{nl/nl}$ mice and *n* = 10 *Pkd1*$^{+/+}$ mice. AVF, arteriovenous fistula.

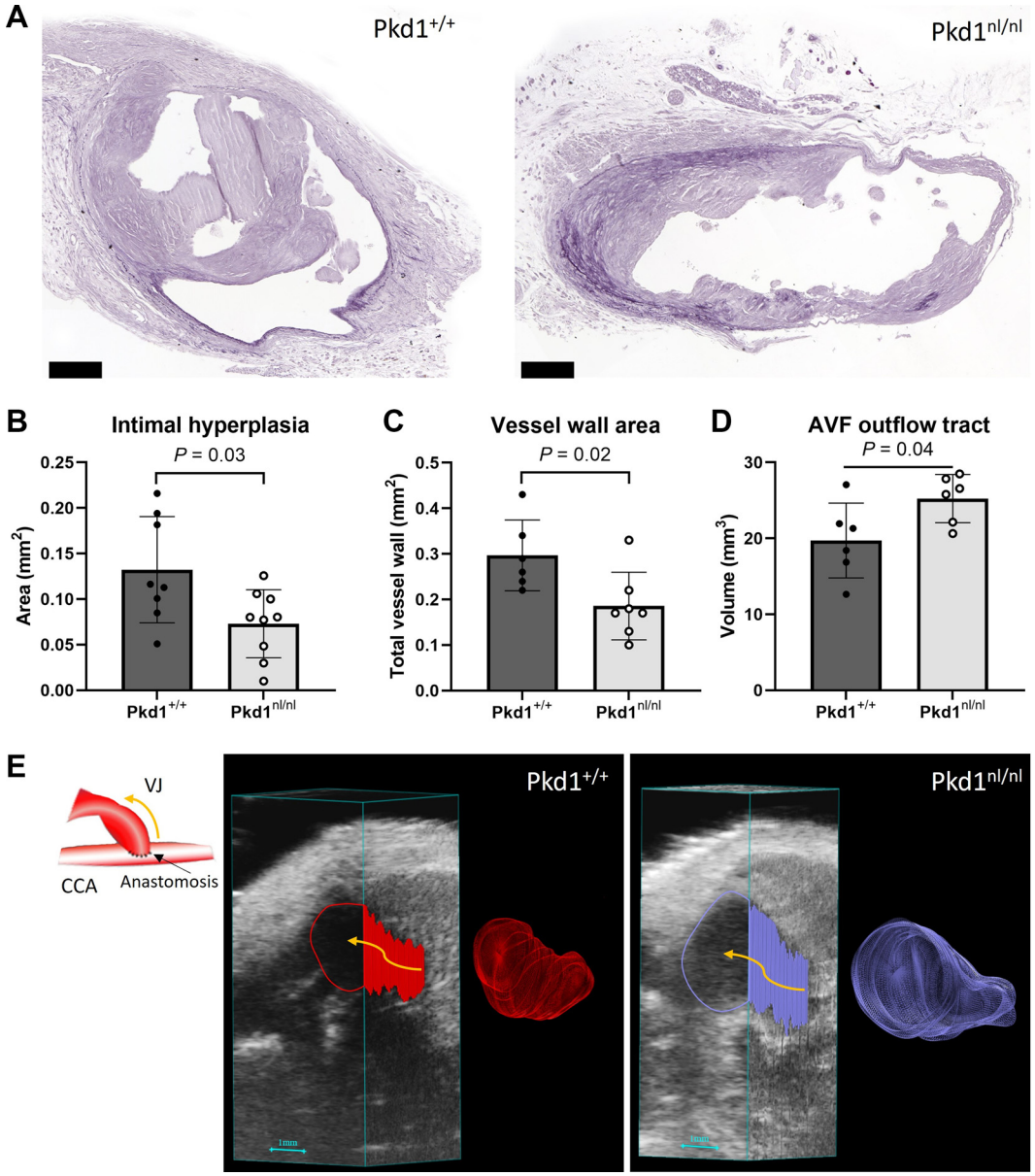

Figure 6. Morphometric analysis of the AVF 21 days postsurgery. *A*: Weigert's Elastin staining of the venous outflow tract representative of *Pkd1*$^{+/+}$ (*left*) and *Pkd1*$^{nl/nl}$ (*right*) mice. The black scale bar indicates 100 µm. *Pkd1*$^{nl/nl}$ mice have decreased intimal hyperplasia formation (*B*), and a smaller vessel wall area (*C*). Analysis of the luminal volume of the AVF outflow tract from ultrasound analysis showed an increased venous luminal volume in *Pkd1*$^{nl/nl}$ AVFs at 21 days post-AVF surgery (*D*). Data are expressed as means ± SD. *E*: visual of the AVF anatomy (*left*) and representative images of volumetric measurements and corresponding 3-D renders of the venous limb of the AVF in *Pkd1*$^{+/+}$ and *Pkd1*$^{nl/nl}$ mice. Volume is standardized over the first 2.5 mm from the anastomosis, represented by the yellow arrow. AVF, arteriovenous fistula; CCA, common carotid artery, VJ, vena jugularis; 3-D, three-dimensional.

Renal Arteries of Patients with ADPKD Show ECM Dysregulation

We obtained renal arteries of patients undergoing a nephrectomy to investigate ECM deposition in the vasculature of patients with ADPKD. Masson trichrome and Weigert's elastin staining (Fig. 8) of the renal arteries of controls with a normal kidney function and patients with ADPKD showed dysregulation of ECM deposition and loss of elastic lamina integrity of the renal artery of patients with chronic kidney failure.

DISCUSSION

In addressing the need for a chronic preclinical model reflective of patients with ESKD undergoing AVF surgery, we utilized an autosomal dominant polycystic kidney disease (ADPKD) model to study AVF maturation in a murine CKD setting.

Pkd1$^{nl/nl}$ mice had increased AVF blood flow, with larger venous outflow tracts. We demonstrated that the increase in luminal AVF volume is due to a combination of increased blood pressure, diminished IH and dysregulated extracellular

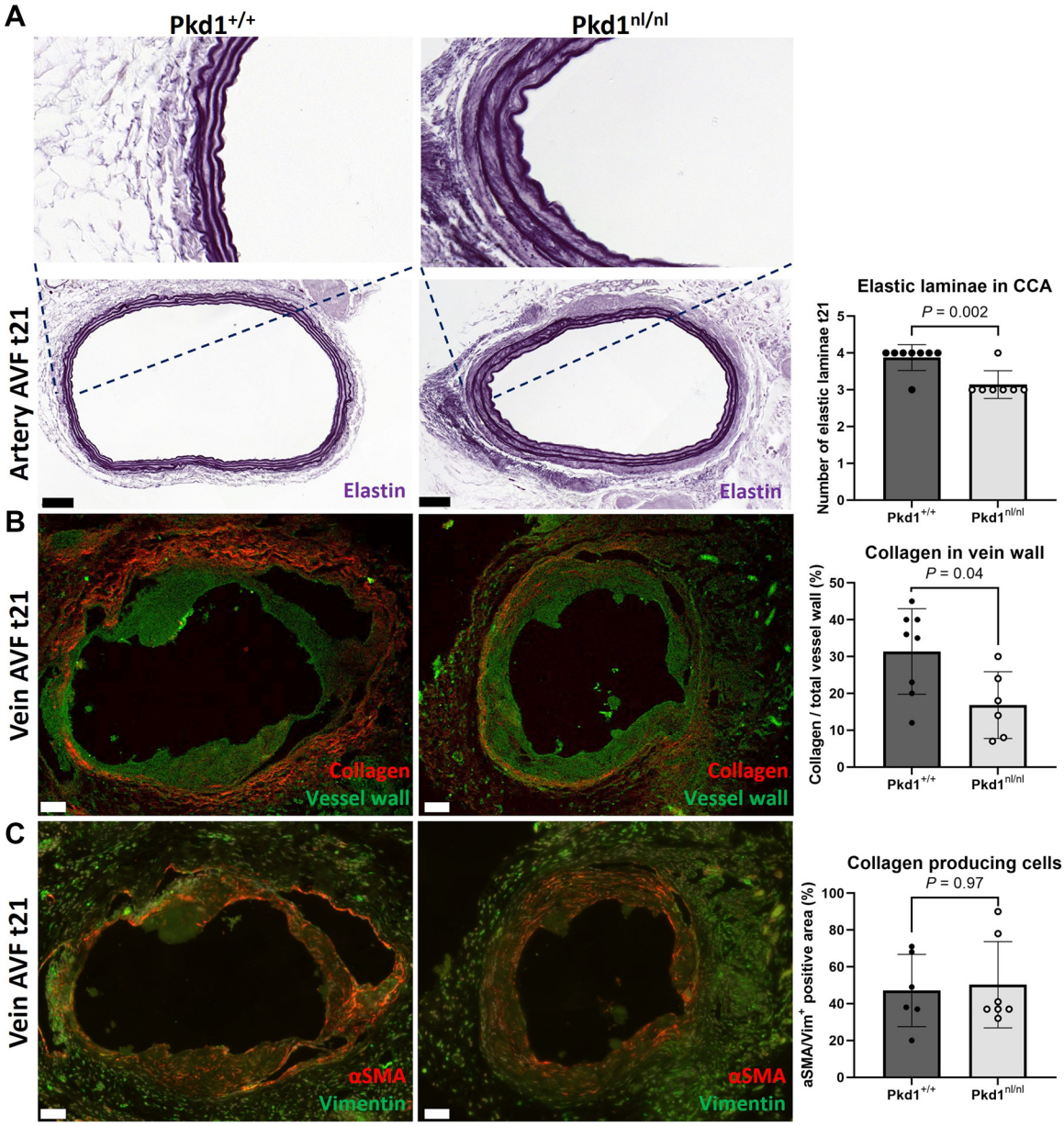

Figure 7. Extracellular matrix protein regulation in murine AVF. Venous and arterial AVF tissue harvested 21 days post-AVF creation. Weigert's elastin stain of the afferent AVF artery (*A*) shows a loss of elastic laminae in the *Pkd1*$^{nl/nl}$ vessel with deposition in between the laminae, top figures are higher magnifications. Second harmonic generation on the venous outflow tract (*B*) showing diminished collagen deposition (band-pass emission filter at 380–430 nm for collagen in red) in the *Pkd1*$^{nl/nl}$ venous outflow tract. The presence of αSMA or Vimentin positive collagen-producing cells was comparable in the venous outflow tract of both groups (*C*). Data are expressed as means ± SD. Scale bar indicates 50 μm. AVF, arteriovenous fistula.

matrix deposition. IPA pathway analysis revealed upregulation of transcription factors Gata6, Sox2, Smarca2, Npm1, and Esrra and cytokines CSF1 and IL-13, suggesting enhanced vascular remodeling, increased (smooth muscle) cellular proliferation, an altered immune response, and metabolic activation in the ADPKD model (16–22). Altered ECM remodeling in mice with ADPKD was observed, both during early remodeling using RNA sequencing, and at the end point of our study on a histological level. *Pkd1*$^{nl/nl}$ AVFs showed downregulation of *Col11A1, Tnc*, *Tnn*, and *Acan* in the first week post-AVF surgery, which are related to ECM interaction and organization (23–26). This was followed at the later time point by disruption of arterial elastin, and decreased venous collagen deposition. The ECM is also proven essential in clinical AVF remodeling: Martinez et al. (27) demonstrated that failed and matured AVFs can be categorized by distinct clusters of differentially expressed ECM components. Pathway enrichment analysis revealed a significant increase in collagen remodeling, both degradation and production, from preaccess veins to pair-matched brachiobasilic AVFs of patients with ESKD. AVF maturation is characterized by phases of ECM degradation, reorganization of the collagen and elastin scaffold, and deposition of ECM proteins (28, 29).

Although murine studies show the importance of hindering elastin deposition (30, 31), direct elastin inhibition in randomized double-blind placebo-controlled trials did not

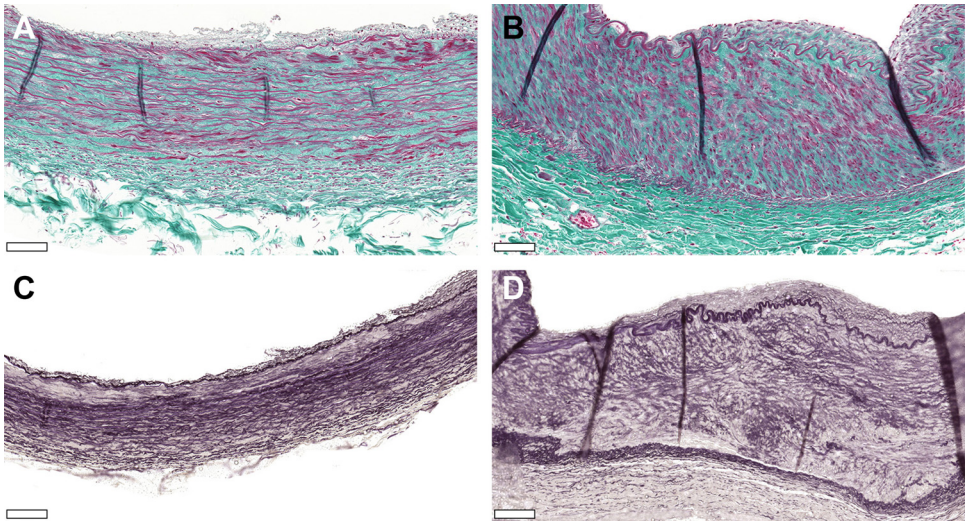

Figure 8. Extracellular matrix in the human renal artery. Masson trichrome staining of a renal artery from a patient with normal kidney function (*A*) and patient with ADPKD (*B*) indicates dysregulated extracellular matrix deposition in human ADPKD vessels. This is also shown by samples stained with Weigert's elastin, where compared with the healthy control (*C*), ADPKD vessels show loss of integrity of the elastin fibers (*D*). Scale bar indicates 100 μm. ADPKD, autosomal dominant polycystic kidney disease; AVF, arteriovenous fistula.

have an effect on AVF venous diameter, stenosis, blood flow, or maturation rates (32, 33). This indicates that solely increasing elastin degradation might not be of therapeutic value to improve maturation and AVF patency. In contrast, inhibiting lysyl oxidase (LOX), which aids crosslinking of collagen and elastin fibers, had beneficial effects on fibrosis, vessel distensibility, and OR of AVFs in rats (34, 35). Concurrently, preaccess veins of patients with ESKD that had higher LOX expression were associated with AVF failure (34). During early AVF remodeling, RNA sequencing analysis showed disturbed venous ECM remodeling, later on followed by decreased collagen expression in the venous outflow tract and disrupted elastin matrix in the afferent artery in *Pkd1*$^{nl/nl}$ mice. This altered vascular remodeling might be essential for the increase in luminal AVF volume, vessel distensibility, and increase in flow. Excessive ECM degradation or inadequate repair, however, can lead to a weakened or even aneurysmal AVF (29), stressing the importance of balanced ECM degradation followed by deposition.

Studying AVF outcomes in other, although more acute, kidney-failure models, Song et al. (36) observed that 5/6th nephrectomy caused vascular fibrosis due to increased myofibroblast differentiation and intimal-ECM. Second, Kang et al. (3) detected increased MMP-9 and TGF-β1 expression in the AVFs in a similar model. Overall, compared with acute renal failure model studies, chronic kidney failure in the form of ADPKD had a differential effect on AVF outcome in general. Surgically or diet-induced loss of kidney function mainly resulted in hindered AVF flow and enhanced formation of IH in rats and mice (2–7, 11, 37). Some attributed AVF failure in their models on EC-related processes such as loss of vascular endothelial-cadherin expression and delayed regeneration of the endothelium (37), oxidative stress (2), and impaired dilatation of both the afferent artery and downstream venous outflow tract (7). Others observed excessive IH formation due to increased VSMC migration and downregulation of contractile VSMC markers α-actin and calponin (5, 11). In our CKD model, however, there was no effect on collagen-producing cells such as VSMCs and fibroblasts. Instead, combined hypertension and uremia resulted in decreased IH formation and ECM deposition, leading to increased AVF venous outflow tract volume and AVF flow.

ADPKD is associated with a higher incidence of aneurysms, mainly intracranial and abdominal (38–41), but also a higher frequency of AVF aneurysms compared with other patients with ESKD has been reported (42). This could be due to altered vasculopathy. 93% of patients with polycystic kidney disease have a mutation in the *PKD1* or *PKD2* gene, encoding polycystin-1 and -2, and the remaining 7% have an undiagnosed mutation or one in a gene involved in polycystin protein regulation.(43–48) Polycystin-1 and -2 interact to form an ion channel complex regulating calcium influx, involved in sensing mechanotransduction and fluid flow (49, 50). *PKD1*, which is affected in our mouse model (12), is expressed in both endothelial cells (ECs) and vascular smooth muscle cells (VSMCs) and is essential to maintain vessel wall integrity (51, 52). Reduced *Pkd1* expression in VSMCs causes the threshold pressure for myogenic contraction to go up (53) and induces phenotypic switching and affects the extracellular matrix (54–56). This can explain the decreased ECM organization in the AVF of *Pkd1*$^{nl/nl}$ mice. It is important to note that we did not observe either venous or arterial AVF aneurysm formation, as there was no significant increase in the diameter of the CCA afferent to the AVF, and we observed a thicker venous wall, strengthened by increased collagen deposition. However, we cannot rule out the possibility of aneurysm formation over a longer time frame. In addition, our model may be influenced by general CKD as well as ADPKD-specific effects, which poses an interesting research question for further studies. Nonetheless, our model is a clinical representative model for a substantial portion of patients with an AVF, as patients with ADPKD comprise ∼9% of patients requiring kidney replacement therapy, and 69% of this patient group undergoes HD (57). The majority of patients with ADPKD on HD utilize an AVF as vascular access (58). The question arises whether the observed differences in AVF remodeling primarily relate to the impaired kidney function or if they are specific for ADPKD. In this respect, it is important to notice that in our recent clinical study, patency rates of AVF/AVG in ADPKD patients were similar to those of patients with ESKD with other primary kidney disease (59). This suggests that

ADPKD does not affect AVF outcomes differently than other causes of ESKD, reinforcing the representativeness of our ADPKD model for patients with ESKD receiving AVFs.

In conclusion, our study introduced a novel in vivo model suitable for studying AVF remodeling in the setting of chronic kidney disease, resulting in improved AVF maturation in mice with ADPKD, as illustrated by enhanced luminal volume and higher AVF flow. Moreover, this ADPKD model holds promise for investigating the effects of hypertension, uremia, and interventions targeting the ECM in AVF remodeling.

DATA AVAILABILITY

Data will be made available upon reasonable request.

SUPPLEMENTAL MATERIAL

Supplemental Figs. S1–S5 and Table S1: https://doi.org/10.6084/m9.figshare.29433362.

DISCLOSURES

No conflicts of interest, financial or otherwise, are declared by the authors.

AUTHOR CONTRIBUTIONS

S.L.L., D.J.P., M.R.d.V., and J.I.R. conceived and designed research; S.L.L., E.P.d.W., J.M.D., and M.R.d.V. performed experiments; S.L.L., E.P.d.W., J.M.D., and J.A.d.K. analyzed data; S.L.L., R.B., M.R.d.V., and J.I.R. interpreted results of experiments; S.L.L., E.P.d.W., and J.A.d.K. prepared figures; S.L.L. drafted manuscript; S.L.L., D.J.P., E.P.d.W., M.R.d.V., and J.I.R. edited and revised manuscript; S.L.L., D.J.P., R.B., E.P.d.W., J.M.D., J.A.d.K., M.R.d.V., and J.I.R. approved final version of manuscript.

REFERENCES

1. **Shiu YT**, **Rotmans JI**, **Geelhoed WJ**, **Pike DB**, **Lee T.** Arteriovenous conduits for hemodialysis: how to better modulate the pathophysiological vascular response to optimize vascular access durability. *Am J Physiol Renal Physiol* 316: F794–F806, 2019. doi:10.1152/ajprenal.00440.2018.
2. **Geenen IL**, **Kolk FF**, **Molin DG**, **Wagenaar A**, **Compeer MG**, **Tordoir JH**, **Schurink GW**, **De Mey JG**, **Post MJ.** Nitric oxide resistance reduces arteriovenous fistula maturation in chronic kidney disease in rats. *PLoS One* 11: e0146212, 2016. doi:10.1371/journal.pone.0146212.
3. **Kang L**, **Grande JP**, **Hillestad ML**, **Croatt AJ**, **Barry MA**, **Katusic ZS**, **Nath KA.** A new model of an arteriovenous fistula in chronic kidney disease in the mouse: beneficial effects of upregulated heme oxygenase-1. *Am J Physiol Renal Physiol* 310: F466–F476, 2016. doi:10.1152/ajprenal.00288.2015.
4. **Zheng C**, **Zhou Y**, **Huang C**, **Zhang Z**, **Liu Y**, **Xu Y.** Establishment of a rat autogenous arteriovenous fistula model following 5/6 nephrectomy. *Exp Ther Med* 10: 219–224, 2015. doi:10.3892/etm.2015.2451.
5. **Ferrer LM**, **Monroy AM**, **Lopez-Pastrana J**, **Nanayakkara G**, **Cueto R**, **Li YF**, **Li X**, **Wang H**, **Yang XF**, **Choi ET.** Caspase-1 plays a critical role in accelerating chronic kidney disease-promoted neointimal hyperplasia in the carotid artery. *J Cardiovasc Transl Res* 9: 135–144, 2016. doi:10.1007/s12265-016-9683-3.
6. **Croatt AJ**, **Grande JP**, **Hernandez MC**, **Ackerman AW**, **Katusic ZS**, **Nath KA.** Characterization of a model of an arteriovenous fistula in the rat: the effect of L-NAME. *Am J Pathol* 176: 2530–2541, 2010. doi:10.2353/ajpath.2010.090649.
7. **Langer S**, **Kokozidou M**, **Heiss C**, **Kranz J**, **Kessler T**, **Paulus N**, **Krüger T**, **Jacobs MJ**, **Lente C**, **Koeppel TA.** Chronic kidney disease aggravates arteriovenous fistula damage in rats. *Kidney Int* 78: 1312–1321, 2010. doi:10.1038/ki.2010.353.
8. **Khattri RB**, **Kim K**, **Anderson EM**, **Fazzone B**, **Harland KC**, **Hu Q**, **Palzkill VR**, **Cort TA**, **O'Malley KA**, **Berceli SA**, **Scali ST**, **Ryan TE.** Metabolomic profiling reveals muscle metabolic changes following iliac arteriovenous fistula creation in mice. *Am J Physiol Renal Physiol* 323: F577–F589, 2022. doi:10.1152/ajprenal.00156.2022.
9. **Rezapour M**, **Khavanin Zadeh M**, **Sepehri MM**, **Alborzi M.** Less primary fistula failure in hypertensive patients. *J Hum Hypertens* 32: 311–318, 2018. doi:10.1038/s41371-018-0052-3.
10. **Wang K**, **Zelnick LR**, **Imrey PB**, **deBoer IH**, **Himmelfarb J**, **Allon MD**, **Cheung AK**, **Dember LM**, **Roy-Chaudhury P**, **Vazquez MA**, **Kusek JW**, **Feldman HI**, **Beck GJ**, **Kestenbaum B**; **The Hemodialysis Fistula Maturation Study Group.** Effect of anti-hypertensive medication history on arteriovenous fistula maturation outcomes. *Am J Nephrol* 48: 56–64, 2018. doi:10.1159/000491828.
11. **Kokubo T**, **Ishikawa N**, **Uchida H**, **Chasnoff SE**, **Xie X**, **Mathew S**, **Hruska KA**, **Choi ET.** CKD accelerates development of neointimal hyperplasia in arteriovenous fistulas. *J Am Soc Nephrol* 20: 1236–1245, 2009. doi:10.1681/ASN.2007121312.
12. **Happé H**, **van der Wal AM**, **Salvatori DCF**, **Leonhard WN**, **Breuning MH**, **de Heer E**, **Peters DJM.** Cyst expansion and regression in a mouse model of polycystic kidney disease. *Kidney Int* 83: 1099–1108, 2013. doi:10.1038/ki.2013.13.
13. **Lantinga-van Leeuwen IS**, **Dauwerse JG**, **Baelde HJ**, **Leonhard WN**, **van de Wal A**, **Ward CJ**, **Verbeek S**, **Deruiter MC**, **Breuning MH**, **de Heer E**, **Peters DJ.** Lowering of Pkd1 expression is sufficient to cause polycystic kidney disease. *Hum Mol Genet* 13: 3069–3077, 2004. doi:10.1093/hmg/ddh336.
14. **Wong CY**, **de Vries MR**, **Wang Y**, **van der Vorst JR**, **Vahrmeijer AL**, **van Zonneveld AJ**, **Roy-Chaudhury P**, **Rabelink TJ**, **Quax PH**, **Rotmans JI.** Vascular remodeling and intimal hyperplasia in a novel murine model of arteriovenous fistula failure. *J Vasc Surg* 59: 192–201.e1, 2014. doi:10.1016/j.jvs.2013.02.242.
15. **Laboyrie SL**, **de Vries M**, **de Jong A**, **de Boer HC Lalai RA**, **Martinez L**, **Vazquez-Padron RI**, **Rotmans JI.** von Willebrand factor: a central regulator of arteriovenous fistula maturation through smooth muscle cell proliferation and outward remodeling. *J Am Heart Assoc* 11: e024581, 2022. doi:10.1161/JAHA.121.024581.
16. **Kopp JL**, **Ormsbee BD**, **Desler M**, **Rizzino A.** Small increases in the level of Sox2 trigger the differentiation of mouse embryonic stem cells. *Stem Cells* 26: 903–911, 2008. doi:10.1634/stemcells.2007-0951.
17. **Yin F**, **Herring BP.** GATA-6 can act as a positive or negative regulator of smooth muscle-specific gene expression. *J Biol Chem* 280: 4745–4752, 2005. doi:10.1074/jbc.M411585200.
18. **Wu W**, **Bao W**, **Chen X**, **Lu Y**, **Fang J**, **Liu J**, **Peng S**, **Pi J**, **Tomlinson B**, **Chan P**, **Zhang Q**, **Zhang L**, **Liu Z**, **Liu J**, **Zhang Y**, **Zhuang T.** Endothelial Gata6 deletion reduces monocyte recruitment and proinflammatory macrophage formation and attenuates atherosclerosis through Cmpk2-Nlrp3 pathways. *Redox Biol* 64: 102775, 2023 [Erratum in *Redox Biol* 66: 102854, 2023]. doi:10.1016/j.redox.2023.102854.
19. **Liu H**, **Zhao Y**, **Zhao G**, **Deng Y**, **Chen YE**, **Zhang J.** SWI/SNF complex in vascular smooth muscle cells and its implications in cardiovascular pathologies. *Cells* 13: 168, 2024. doi:10.3390/cells13020168.
20. **Rao C**, **Liu B**, **Huang D**, **Chen R**, **Huang K**, **Li F**, **Dong N.** Nucleophosmin contributes to vascular inflammation and endothelial dysfunction in atherosclerosis progression. *J Thorac Cardiovasc Surg* 161: e377–e393, 2021. doi:10.1016/j.jtcvs.2019.10.152.
21. **Sopariwala DH**, **Likhite N**, **Pei G**, **Haroon F**, **Lin L**, **Yadav V**, **Zhao Z**, **Narkar VA.** Estrogen-related receptor α is involved in angiogenesis and skeletal muscle revascularization in hindlimb ischemia. *FASEB J* 35: e21480, 2021 [Erratum in *FASEB J* 35: e21887, 2021]. doi:10.1096/fsb2.21887.
22. **Sumi D**, **Ignarro LJ.** Estrogen-related receptor alpha 1 up-regulates endothelial nitric oxide synthase expression. *Proc Natl Acad Sci USA* 100: 14451–14456, 2003. doi:10.1073/pnas.2235590100.
23. **Sun M**, **Luo EY**, **Adams SM**, **Adams T**, **Ye Y**, **Shetye SS**, **Soslowsky LJ**, **Birk DE.** Collagen XI regulates the acquisition of collagen fibril structure, organization and functional properties in tendon. *Matrix Biol* 94: 77–94, 2020. doi:10.1016/j.matbio.2020.09.001.
24. **Giuffrida A**, **Scarpa S**, **Birarelli P**, **Modesti A.** The interaction of tenascin-C with fibronectin modulates the migration and specific metalloprotease activity in human mesothelioma cell lines of

different histotype. *Int J Oncol* 25: 745–750, 2004. doi:10.3892/ijo.25.3.745.

25. **Jones PL**, **Jones FS**, **Zhou B**, **Rabinovitch M.** Induction of vascular smooth muscle cell tenascin-C gene expression by denatured type I collagen is dependent upon a beta3 integrin-mediated mitogen-activated protein kinase pathway and a 122-base pair promoter element. *J Cell Sci* 112: 435–445, 1999. doi:10.1242/jcs.112.4.435.
26. **Suna G**, **Wojakowski W**, **Lynch M**, **Barallobre-Barreiro J**, **Yin X**, **Mayr U**, **Baig F**, **Lu R**, **Fava M**, **Hayward R**, **Molenaar C**, **White SJ**, **Roleder T**, **Milewski KP**, **Gasior P**, **Buszman PP**, **Buszman P**, **Jahangiri M**, **Shanahan CM**, **Hill J**, **Mayr M.** Extracellular matrix proteomics reveals interplay of aggrecan and aggrecanases in vascular remodeling of stented coronary arteries. *Circulation* 137: 166–183, 2018. doi:10.1161/CIRCULATIONAHA.116.023381.
27. **Martinez L**, **Rojas MG**, **Tabbara M**, **Pereira-Simon S**, **Falcon NS**, **Rauf MA**, **Challa AS**, **Zigmond ZM**, **Griswold AJ**, **Duque JC**, **Lassance-Soares RM**, **Velazquez OC**, **Salman LH**, **Vazquez-Padron RI.** The transcriptomics of the human vein transformation after arteriovenous fistula anastomosis uncovers layer-specific remodeling and hallmarks of maturation failure. *Kidney Int Rep* 8: 837–850, 2023. doi:10.1016/j.ekir.2023.01.008.
28. **Hall MR**, **Yamamoto K**, **Protack CD**, **Tsuneki M**, **Kuwahara G**, **Assi R**, **Brownson KE**, **Bai H**, **Madri JA**, **Dardik A.** Temporal regulation of venous extracellular matrix components during arteriovenous fistula maturation. *J Vasc Access* 16: 93–106, 2015. doi:10.5301/jva.5000290.
29. **Laboyrie SL**, **de Vries MR**, **Bijkerk R**, **Rotmans JI.** Building a scaffold for arteriovenous fistula maturation: unravelling the role of the extracellular matrix. *Int J Mol Sci* 24: 10825, 2023. doi:10.3390/ijms241310825.
30. **Wong CY**, **Rothuizen TC**, **de Vries MR**, **Rabelink TJ**, **Hamming JF**, **van Zonneveld AJ**, **Quax PH**, **Rotmans JI.** Elastin is a key regulator of outward remodeling in arteriovenous fistulas. *Eur J Vasc Endovasc Surg* 49: 480–486, 2015. doi:10.1016/j.ejvs.2014.12.035.
31. **Bezhaeva T**, **de Vries MR**, **Geelhoed WJ**, **van der Veer EP**, **Versteeg S**, **van Alem CMA**, **Voorzaat BM**, **Eijkelkamp N**, **van der Bogt KE**, **Agoulnik AI**, **van Zonneveld AJ**, **Quax PHA**, **Rotmans JI.** Relaxin receptor deficiency promotes vascular inflammation and impairs outward remodeling in arteriovenous fistulas. *FASEB J* 32: 6293–6304, 2018. doi:10.1096/fj.201800437R.
32. **Peden EK**, **Lucas JF**, **Browne BJ**, **Settle SM**, **Scavo VA**, **Bleyer AJ**, **Ozaki CK**, **Teruya TH**, **Wilson SE**, **Mishler RE**, **Ferris BL**, **Hendon KS**, **Moist L**, **Dixon BS**, **Wong MD**, **Magill M**, **Lindow F**, **Gustafson P**, **Burke SK**; **PATENCY-2 Investigators.** PATENCY-2 trial of vonapanitase to promote radiocephalic fistula use for hemodialysis and secondary patency. *J Vasc Access* 23: 265–274, 2022. doi:10.1177/1129729820985626.
33. **Bleyer AJ**, **Scavo VA**, **Wilson SE**, **Browne BJ**, **Ferris BL**, **Ozaki CK**, **Lee T**, **Peden EK**, **Dixon BS**, **Mishler R**, **O'Connor TP**, **Kidd K**, **Burke SK**; **PATENCY-1 Investigators.** A randomized trial of vonapanitase (PATENCY-1) to promote radiocephalic fistula patency and use for hemodialysis. *J Vasc Surg* 69: 507–515, 2019 [Erratum in *J Vasc Surg* 69: 1329, 2019]. doi:10.1016/j.jvs.2019.01.042.
34. **Hernandez DR**, **Applewhite B**, **Martinez L**, **Laurito T**, **Tabbara M**, **Rojas MG**, **Wei Y**, **Selman G**, **Knysheva M**, **Velazquez OC**, **Salman LH**, **Andreopoulos FM**, **Shiu YT**, **Vazquez-Padron RI.** Inhibition of lysyl oxidase with β-aminopropionitrile improves venous adaptation after arteriovenous fistula creation. *Kidney360* 2: 270–278, 2021. doi:10.34067/KID.0005012020.
35. **Applewhite B**, **Gupta A**, **Wei Y**, **Yang X**, **Martinez L**, **Rojas MG**, **Andreopoulos F**, **Vazquez-Padron RI.** Periadventitial β-aminopropionitrile-loaded nanofibers reduce fibrosis and improve arteriovenous fistula remodeling in rats. *Front Cardiovasc Med* 10: 1124106, 2023. doi:10.3389/fcvm.2023.1124106.
36. **Song K**, **Qing Y**, **Guo Q**, **Peden EK**, **Chen C**, **Mitch WE**, **Truong L**, **Cheng J.** PDGFRA in vascular adventitial MSCs promotes neointima formation in arteriovenous fistula in chronic kidney disease. *JCI Insight* 5: e137298, 2020. doi:10.1172/jci.insight.137298.
37. **Liang A**, **Wang Y**, **Han G**, **Truong L**, **Cheng J.** Chronic kidney disease accelerates endothelial barrier dysfunction in a mouse model of an arteriovenous fistula. *Am J Physiol Renal Physiol* 304: F1413–F1420, 2013. doi:10.1152/ajprenal.00585.2012.
38. **Cagnazzo F**, **Gambacciani C**, **Morganti R**, **Perrini P.** Intracranial aneurysms in patients with autosomal dominant polycystic kidney disease: prevalence, risk of rupture, and management. A systematic review. *Acta Neurochir (Wien)* 159: 811–821, 2017. doi:10.1007/s00701-017-3142-z.
39. **Sung PH**, **Yang YH**, **Chiang HJ**, **Chiang JY**, **Chen CJ**, **Liu CT**, **Yu CM**, **Yip HK.** Risk of aortic aneurysm and dissection in patients with autosomal-dominant polycystic kidney disease: a nationwide population-based cohort study. *Oncotarget* 8: 57594–57604, 2017. doi:10.18632/oncotarget.16338.
40. **Kato A**, **Takita T**, **Furuhashi M**, **Maruyama Y**, **Hishida A.** Abdominal aortic aneurysms in hemodialysis patients with autosomal dominant polycystic kidney disease. *Nephron* 88: 185–186, 2001. doi:10.1159/000045984.
41. **Irazabal MV**, **Huston J III**, **Kubly V**, **Rossetti S**, **Sundsbak JL**, **Hogan MC**, **Harris PC**, **Brown RD Jr**, **Torres VE.** Extended follow-up of unruptured intracranial aneurysms detected by presymptomatic screening in patients with autosomal dominant polycystic kidney disease. *Clin J Am Soc Nephrol* 6: 1274–1285, 2011. doi:10.2215/CJN.09731110.
42. **Jankovic A**, **Donfrid B**, **Adam J**, **Ilic M**, **Djuric Z**, **Damjanovic T**, **Popovic J**, **Popovic G**, **Radojicic Z**, **Dimkovic N.** Arteriovenous fistula aneurysm in patients on regular hemodialysis: prevalence and risk factors. *Nephron Clin Pract* 124: 94–98, 2013. doi:10.1159/000355548.
43. Polycystic kidney disease: the complete structure of the PKD1 gene and its protein. The International Polycystic Kidney Disease Consortium. *Cell* 81: 289–298, 1995. doi:10.1016/0092-8674(95)90339-9.
44. **Mochizuki T**, **Wu G**, **Hayashi T**, **Xenophontos SL**, **Veldhuisen B**, **Saris JJ**, **Reynolds DM**, **Cai Y**, **Gabow PA**, **Pierides A**, **Kimberling WJ**, **Breuning MH**, **Deltas CC**, **Peters DJ**, **Somlo S.** PKD2, a gene for polycystic kidney disease that encodes an integral membrane protein. *Science* 272: 1339–1342, 1996. doi:10.1126/science.272.5266.1339.
45. **Senum SR**, **Li YSM**, **Benson KA**, **Joli G**, **Olinger E**, **Lavu S**, **Madsen CD**, **Gregory AV**, **Neatu R**, **Kline TL**, **Audrézet MP**, **Outeda P**, **Nau CB**, **Meijer E**, **Ali H**, **Steinman TI**, **Mrug M**, **Phelan PJ**, **Watnick TJ**, **Peters DJM**, **Ong ACM**, **Conlon PJ**, **Perrone RD**, **Cornec-Le Gall E**, **Hogan MC**, **Torres VE**, **Sayer JA**, **Harris PC**; **Genomics England Research Consortium, the HALT PKD, CRISP, DIPAK, ADPKD Modifier, and TAME PKD studies.** Monoallelic IFT140 pathogenic variants are an important cause of the autosomal dominant polycystic kidney-spectrum phenotype. *Am J Human Genetics* 109: 136–156, 2022. doi:10.1016/j.ajhg.2021.11.016.
46. **Cornec-Le Gall E**, **Olson RJ**, **Besse W**, **Heyer CM**, **Gainullin VG**, **Smith JM**, **Audrézet MP**, **Hopp K**, **Porath B**, **Shi B**, **Baheti S**, **Senum SR**, **Arroyo J**, **Madsen CD**, **Férec C**, **Joly D**, **Jouret F**, **Fikri-Benbrahim O**, **Charasse C**, **Coulibaly JM**, **Yu AS**, **Khalili K**, **Pei Y**, **Somlo S**, **Le Meur Y**, **Torres VE**, **Harris PC**; **Consortium for Radiologic Imaging Studies of Polycystic Kidney Disease.** Monoallelic mutations to DNAJB11 cause atypical autosomal-dominant polycystic kidney disease. *Am J Hum Genet* 102: 832–844, 2018. doi:10.1016/j.ajhg.2018.03.013.
47. **Porath B**, **Gainullin VG**, **Cornec-Le Gall E**, **Dillinger EK**, **Heyer CM**, **Hopp K**, **Edwards ME**, **Madsen CD**, **Mauritz SR**, **Banks CJ**, **Baheti S**, **Reddy B**, **Herrero JI**, **Bañales JM**, **Hogan MC**, **Tasic V**, **Watnick TJ**, **Chapman AB**, **Vigneau C**, **Lavainne F**, **Audrézet MP**, **Ferec C**, **Le Meur Y**, **Torres VE**, **Harris PC**; **Consortium for Radiologic Imaging Studies of Polycystic Kidney Disease.** Mutations in GANAB, encoding the glucosidase IIα subunit, cause autosomal-dominant polycystic kidney and liver disease. *Am J Hum Genet* 98: 1193–1207, 2016. doi:10.1016/j.ajhg.2016.05.004.
48. **Besse W**, **Chang AR**, **Luo JZ**, **Triffo WJ**, **Moore BS**, **Gulati A**, **Hartzel DN**, **Mane S**, **Torres VE**, **Somlo S**, **Mirshahi T**; **Regeneron Genetics Center.** ALG9 mutation carriers develop kidney and liver cysts. *J Am Soc Nephrol* 30: 2091–2102, 2019. doi:10.1681/ASN.2019030298.
49. **Hanaoka K**, **Qian F**, **Boletta A**, **Bhunia AK**, **Piontek K**, **Tsiokas L**, **Sukhatme VP**, **Guggino WB**, **Germino GG.** Co-assembly of polycystin-1 and -2 produces unique cation-permeable currents. *Nature* 408: 990–994, 2000. doi:10.1038/35050128.
50. **Nauli SM**, **Alenghat FJ**, **Luo Y**, **Williams E**, **Vassilev P**, **Li X**, **Elia AE**, **Lu W**, **Brown EM**, **Quinn SJ**, **Ingber DE**, **Zhou J.** Polycystins 1 and 2 mediate mechanosensation in the primary cilium of kidney cells. *Nat Genet* 33: 129–137, 2003. doi:10.1038/ng1076.
51. **Kim K**, **Drummond I**, **Ibraghimov-Beskrovnaya O**, **Klinger K**, **Arnaout MA.** Polycystin 1 is required for the structural integrity of blood vessels. *Proc Natl Acad Sci USA* 97: 1731–1736, 2000. doi:10.1073/pnas.040550097.

52. **Griffin MD**, **Torres VE**, **Grande JP**, **Kumar R.** Vascular expression of polycystin. *J Am Soc Nephrol* 8: 616–626, 1997. doi:10.1681/ASN.V84616.
53. **Sharif-Naeini R**, **Folgering JH**, **Bichet D**, **Duprat F**, **Lauritzen I**, **Arhatte M**, **Jodar M**, **Dedman A**, **Chatelain FC**, **Schulte U**, **Retailleau K**, **Loufrani L**, **Patel A**, **Sachs F**, **Delmas P**, **Peters DJM**, **Honoré E.** Polycystin-1 and -2 dosage regulates pressure sensing. *Cell* 139: 587–596, 2009. doi:10.1016/j.cell.2009.08.045.
54. **Zhang J**, **Liu F**, **He YB**, **Zhang W**, **Ma WR**, **Xing J**, **Wang LX.** Polycystin-1 downregulation induced vascular smooth muscle cells phenotypic alteration and extracellular matrix remodeling in thoracic aortic dissection. *Front Physiol* 11: 548055, 2020. doi:10.3389/fphys.2020.548055.
55. **Mangos S**, **Lam PY**, **Zhao A**, **Liu Y**, **Mudumana S**, **Vasilyev A**, **Liu A**, **Drummond IA.** The ADPKD genes pkd1a/b and pkd2 regulate extracellular matrix formation. *Dis Model Mech* 3: 354–365, 2010. doi:10.1242/dmm.003194.
56. **Drummond IA.** Polycystins, focal adhesions and extracellular matrix interactions. *Biochim Biophys Acta* 1812: 1322–1326, 2011. doi:10.1016/j.bbadis.2011.03.003.
57. **Astley ME**, **Boenink R**, **ElHafeez SA**, **Trujillo-Alemán S**, **Arribas F**, **Åsberg A**, **et al.** The ERA Registry Annual Report 2020: a summary. *Clin Kidney J* 16: 1330–1354, 2023. doi:10.1093/ckj/sfad087.
58. **Budhram B**, **Akbari A**, **Brown P**, **Biyani M**, **Knoll G**, **Zimmerman D**, **Edwards C**, **McCormick B**, **Bugeja A**, **Sood MM.** End-stage kidney disease in patients with autosomal dominant polycystic kidney disease: a 12-year study based on the Canadian Organ Replacement Registry. *Can J Kidney Health Dis* 5: 2054358118778568, 2018. doi:10.1177/2054358118778568.
59. **Laboyrie SL**, **Svensson MK**, **Josemans S**, **Sigvant B**, **Rotmans JI**, **Welander G.** Vascular access outcomes in patients with autosomal dominant polycystic kidney disease. *Kidney360* 5: 877–885, 2024. doi:10.34067/KID.0000000000000453.